Cryoelectron Microscopy of Low Density Lipoprotein in Vitreous Ice

Joshua M. Spin and David Atkinson
Department of Biophysics, Boston University School of Medicine, Center for Advanced Biomedical Research, Boston Massachusetts 02118 USA

ABSTRACT In this report, images of low density lipoprotein (LDL) in vitreous ice at ~30 Å resolution are presented. These images show that LDL is a quasi-spherical particle, ~220–240 Å in diameter, with a region of low density (lipid) surrounded by a ring (in projection) of high density believed to represent apolipoprotein B-100. This ring is seen to be composed of four or five (depending on view) large regions of high density material that may represent protein superdomains. Analysis of LDL images obtained at slightly higher magnification reveals that areas of somewhat lower density connect these regions, in some cases crossing the projectional interiors of the LDL particles. Preliminary image analysis of LDL covalently labeled at Cys3734 and Cys4190 with 1.4-nm Nanogold clusters demonstrates that this methodology will provide an important site-specific marker in studies designed to map the organization of apoB at the surface of LDL.

INTRODUCTION

Low density lipoprotein (LDL) is a macromolecular assembly of lipids and proteins that serves as the primary transport particle for cholesterol in human plasma (Brown and Goldstein, 1976). LDL has been associated positively with the development of atherosclerosis (Gofman et al., 1954; Kannel et al., 1971; Sniderman et al., 1980). Physicochemical methods have established a microemulsion model for the quasi-spherical structure of the LDL particle. In this model, a neutral core of cholesteryl esters and triglyceride is surrounded and surface-stabilized by an amphipathic monolayer containing polar phospholipids, cholesterol, and one molecule of apolipoprotein B-100 (apoB) (Atkinson et al., 1977; Deckelbaum et al., 1975; Ginsburg et al., 1982).

The structure of apoB on the particle surface helps to determine the roughly spherical structure of LDL, and is crucial to both the formation and function of the particle (Yang et al., 1986, 1989). ApoB is a ~550,000 molecular weight glycoprotein with 4536 amino acids and is one of the largest monomeric proteins known (Cladaras et al., 1986; Knott et al., 1986; Yang et al., 1986). In addition to its structural role in stabilizing the particle, apoB serves as the ligand for the LDL receptor on cell surfaces (Basu et al., 1977; Mahley and Innerarity, 1978). The organization of apoB on the surface of LDL has been explored by a number of methods including negative stain electron microscopy coupled with anti-apoB monoclonal antibodies of known epitope (Chatterton et al., 1991), and trypsin digestion (Yang et al., 1989). However, the surface structure of LDL and the conformation of apoB at the particle surface remain largely undetermined.

In this study, cryoelectron microscopy, which closely maintains the natural hydrated environment of macromolecules (Dubochet et al., 1987; Adrian et al., 1984), has been used to investigate the structure of the LDL particle and the disposition of apoB at its surface (Atkinson, 1988; Spin and Atkinson, 1993). Direct observation of the specimen at low electron dose in vitreous ice is a relatively new method that removes many of the artifacts associated with negative staining, such as dessication, high dose radiation damage, and the need to rely on staining patterns for data. However, low electron dose means a low signal-to-noise ratio, and lack of stain results in images that are formed largely by phase contrast rather than amplitude contrast (Dubochet et al., 1987; Erickson and Klug, 1971). Image processing techniques have been developed to overcome some of these difficulties (Frank et al., 1981).

To begin mapping apoB at the surface of LDL, we have developed methods for site-specific gold labeling of the two free and surface-accessible cysteine residues (Cys-22 (3734) and Cys-24 (4190)) of apoB (Coleman et al., 1989; Sommer et al., 1991; Yang et al., 1990). Our goal is to obtain independent projectional views of apoB on LDL that may be processed to give three-dimensional surface models of the particle. In this report, we present initial two-dimensional projectional images of the LDL particle.

MATERIALS AND METHODS

General methods

KBr, sodium azide (NaN_3), NaCl, Na_2CO_3, $NaHCO_3$, DMSO, and EDTA were obtained from Fisher Scientific (Fair Lawn, NJ). Ferritin was supplied by Sigma Chemical Co. (St. Louis, MO). Sodium phosphotungstate (NaPT) was supplied by Ladd Research Industries, Inc. (Burlington, VT). Copper EM grids, 200-mesh Gilder and 400-mesh Gilder or Vecco, and carbon rods were supplied by Electron Microscopy Sciences (Fort Washington, PA), Ernest F. Fullam, Inc. (Latham, NY), and Ted Pella, Inc. (Redding, CA). SO-163 EM film was obtained from Eastman Kodak (Rochester, NY). Precast agarose gels were obtained from Ciba Corning Diagnostics Corp. (Palo Alto, CA). Centrifuge tubes were supplied by Nalge Company (Rochester, NY) and Beckman Instruments (Palo Alto, CA).

Received for publication 13 May 1994 and in final form 27 February 1995.
Address reprint requests to Dr. David Atkinson, Department of Biophysics, Boston University School of Medicine, Center for Advanced Biomedical Research, Boston, MA 02118-2394. Tel.: 617-638-4001; Fax: 617-638-4041; E-mail: atkinson@med-biophi.bu.edu.

0006-3495/95/05/2115/09 $2.00

LDL isolation and preparation

Plasma was isolated from blood freshly drawn from normal volunteers at University Hospital of Boston. The donors were members of our laboratory whose LDL contained only the B-100 form of apoB (Cardin et al., 1984). EDTA and NaN_3 were added to the plasma to concentrations of 0.01 and 0.005%, respectively. LDL was isolated at 1.025–1.050 g/ml salt density (addition of solid KBr) by sequential ultracentrifugation (Havel et al., 1955) in 70 Ti clear screwtop ultracentrifuge tubes. LDL was washed by ultracentrifugal flotation through an overlaying $d = 1.063$ g/ml KBr solution. Spins were performed in a L8–70 (or L8–70 M) ultracentrifuge (Beckman Instruments) at 55,000 rpm in a 70 Ti rotor for 16 h at 5°C. The LDL was dialyzed for 24 h against three changes of 4 l of 50 mM Na carbonate, 50 mM NaCl, 0.02% NaN_3, pH 10.0 at 4°C. The purity and oxidation level of the LDL fraction was confirmed using agarose gel electrophoresis (Noble, 1968) staining with Coomassie Brilliant Blue and Sudan Black B.

To increase LDL homogeneity for Nanogold (Nanoprobes, Inc., Stony Brook, NY) labeling studies, samples were subjected to density gradient fractionation. After a flotation at $d = 1.025$ g/ml, the bottom fraction of the tube was adjusted to $d = 1.050$ g/ml with KBr. This solution was used as the bottom layer in a salt solution density gradient (Redgrave et al., 1975) with $d = 1.040/1.030/1.020$ g/ml (KBr dissolved in Na carbonate solution) layered sequentially into 2″×0.5″ clear ultracentrifuge tubes. A control tube was prepared using $d = 1.050$ g/ml (KBr in Na carbonate solution) as the bottom fraction. The gradient was ultracentrifuged for 20 h at 50,000 rpm and 20°C in an SW-55 rotor. Refractive index measurements were taken for control tube fractions. These measurements provided density values for sample tube fraction volumes. Sample tube fractions were evaluated for their LDL content and oxidation level by agarose gel electrophoresis. ApoB concentration was measured by DC protein assay (Bio-Rad Laboratories, Melville, NY) (Lowry et al., 1951; Peterson, 1979). Particle size distribution was determined by negative stain electron microscopy (1% NaPT, pH 7.4).

The LDL in the density gradient fractions contained a narrow, approximately symmetrical population distribution with a single peak in the range $1.020 < d < 1.040$ g/ml. The peak contained pure, nonoxidized, homogenous LDL ($1.029 < d < 1.031$ g/ml) of diameter 255 ± 10 Å as measured directly from micrographs of negatively stained particles. These fractions were pooled and concentrated in Centricon microconcentrators (Amicon, Inc., Beverly, MA) to ~1.3–1.9 mg/ml protein.

A Macra Lp(a) Enzyme Immunoassay Kit (Terumo Medical Corporation, Elkton, MD) was used to perform an ELISA for lipoprotein-a (Lp(a)) on the donor plasma, on the LDL purified by sequential ultracentrifugation, and on the LDL obtained by density gradient to establish that there was no significant contamination of the LDL population by this particle. The donor plasma contained few Lp(a), with a ratio of Lp(a) to total apoB of 1:7.623 (protein measured by DC protein assay). After the ultracentrifugations, Lp(a) levels dropped below the detection threshold of the assay.

Nanogold labeling of LDL

The two free cysteine residues of apoB-100 located at positions 3734 and 4190 (Coleman et al., 1989; Sommer et al., 1991; Yang et al., 1990) were labeled with 55 gold atom clusters with 1.4-nm gold cores (Nanogold) (Furuya et al., 1991; Hainfeld and Furuya, 1992). This gold label is available as a monomaleimido derivative and is designed to bind covalently and irreversibly to sulfhydryls.

The gold reagent was dissolved in 100 μl of DMSO. Deionized reverse osmosis-purified water was added to activate the reagent and provide appropriate buffer concentrations and pH, giving a final volume of 1 ml after addition of concentrated LDL sample. The gold reagent was available in 10-fold molar excess of that necessary to label both cysteines. The mixture was rocked gently at 4°C for 18–24 h to ensure completion of the reaction, and then centrifuged briefly at 6400 rpm for 2 min to precipitate any particulate matter (excess gold). The supernatant was fractionated on a Sephadex-100 (Pharmacia LKB, Piscataway, NJ) gel filtration column to isolate LDL with bound gold (~2.38×10^6 kDa per LDL particle) from unbound gold (~15,000 kDa per gold cluster). The eluent was 50 mM Na carbonate, 50 mM NaCl, 0.02% NaN_3, pH 10. Preparations containing lower levels of salt tended to contain LDL gathered in strings or clumps when observed in the electron microscope (data not shown).

Gold-labeled LDL was collected in the excluded volume and concentrated in microconcentrators at ~1000 × g at 4°C in an SS-34 rotor to ~0.40–0.60 mg/ml protein. Samples were stored at 4°C under nitrogen for less than a week before cryopreservation for electron microscopy. All cryospecimens were kept between −170 and −180°C.

Cryoelectron microscopy

Ferritin was added to unlabelled LDL samples (final concentration 0.01 mg/ml) to aid in focusing. Tobacco mosaic virus (provided by Dr. Donald Caspar of Brandeis University, Waltham, MA) was added to each gold-labeled LDL sample just before cryopreparation (final concentration 0.525 mg/ml) for use in magnification calibration. LDL was diluted to a final concentration of 0.5–1.0 mg/ml apoB in varying salt solutions. Initial studies were carried out on unlabeled LDL samples that were frozen in 0.15 M NaCl. In later studies on unlabeled LDL, samples were frozen in 0.212 M KBr (also Na carbonate and NaCl in trace amounts). Gold-labeled LDL were frozen in 50 mM Na carbonate, 50 mM NaCl, 0.02% NaN_3, pH 10.

Samples of 5–10 μl were applied to glow-discharged holey carbon films on 200- or 400-mesh copper grid supports, blotted, and plunged immediately into liquid nitrogen-cooled liquid ethane using either a gravity-driven method or a specially designed compressed air-driven plunging apparatus (Dubochet et al., 1987; Lepault et al., 1983; Milligan et al., 1984; Wagenknecht et al., 1990).

Unlabeled LDL were observed initially at 80 kV on a Philips (Eindhoven, The Netherlands) EM420 transmission electron microscope (TEM) at the Molecular Research Council Laboratory for Molecular Biology (Cambridge, U.K.). Later observations of unlabeled LDL were made at 100 kV on a Philips CM12 TEM. Gold-labeled LDL were observed on the CM12. Both microscopes were configured for low dose, with a goniometer, cold stage, and anticontaminator. Model 626 and 636 (Gatan, Inc., Pleasanton, CA) cryotransfer cooling holders and workstations were used. The net electron dose was <10 electrons/Å^2.

Focusing/astigmating was accomplished at 230,000× on carbon at the edges of the holes. Micrographs were taken at 49,000× magnification at a nominal defocus of 2.00 μm (unlabeled LDL, EM420), 60,000× at 2.00 μm (unlabeled LDL, CM12) and 60,000× at 1.75 μm (gold-labeled LDL) to obtain phase contrast. After each exposure, observations were made with a diffraction aperture inserted to ensure that the field contained no nonvitreous ice (e.g., cubic, hexagonal). In the CM12-relative ice thickness comparison, data were collected using the internal computerized light meter.

Image processing and analysis

The micrographs that contained the highest contrast, no or little melting of the vitreous ice, and the fewest artifacts (e.g., surface ice crystals, excess ferritin, etc.) were chosen for scanning.

Micrographs were scanned and digitized using either a raster with resolution ~10 Å/pixel (unlabeled LDL, EM420) or ~5 Å/pixel (gold-labeled LDL) on an Eikonix 1412 digital imaging camera system (Ektron Applied Imaging, Inc., Bedford, MA) controlled by a Sun IPC workstation (Sun Microsystems, Mountain View, CA). Digitized images were displayed for windowing and visual assessment on VAX3100/40 and VAX4000/60 workstations (Digital Equipment Corporation, Maynard, MA). All image processing and manipulation were performed on these workstations using the SPIDER (Frank et al., 1981) software package except where indicated.

Calibration of magnification and particle size of digitized gold-labeled LDL micrographs to exactly 5 Å/pixel was achieved using images of the tobacco mosaic virus that was included with the sample. The Fourier transform of chosen virion images was computed, and the third layer line axial spacing (1/23 Å^{-1}) was used to calculate the size per pixel of the digitized images. These procedures were performed using a suite of image analysis programs for helical objects (Owen and DeRosier, 1993). All scanned micrographs were within 2% of the correct raster and therefore did not require interpolation. To ensure data compatibility between images, the micrograph

image data were floated by dividing the pixel values by the image average and then subtracting 1 from each pixel.

Individual particle images were windowed interactively into image files. Each image was masked with a circular, Gaussian mask with a radial drop off outside the mask of half-intensity every three pixels. The images were padded into 64×64 (unlabeled LDL) or 128×128 (gold-labeled LDL) pixel boxes with a background equivalent to that at the mask edge. Images were checked visually to ensure clarity and particle completeness.

Particles were centered in the window by iterative Fourier space translational alignment procedures that were developed and tested on both real images of LDL and artificially generated images resembling LDL in shape, size, and character. Procedures employing rotational averaging and edge detection methods were developed using SPIDER routines, to measure the radius of each particle.

RESULTS

Unlabeled LDL

A field of unlabeled human LDL in vitreous ice is shown in Fig. 1. The background is essentially free of breakdown products, but the small ferritin complexes are visible as a small ring of protein with 0–4 iron complexes inside. A few surface ice crystals may be seen. The LDL are visible as ovoid-to-circular projectional views, with dark (higher density) areas around the edges and occasionally through the center. The projections of LDL particles often appear somewhat egg-shaped, with a small area of high density at the pointed end. In projection this region appears to protrude somewhat from the edge of the particle and in some images appears to be extending away from the edge of the particle. The higher density areas of the LDL are uneven and often consist of small dense regions visibly connected by areas of slightly lower density. A second field of unlabeled LDL obtained under different salt conditions (0.212 M KBr) is shown in Fig. 2. Characteristics are similar to those for LDL in 0.15 M NaCl (Fig. 1); however, contrast is improved, with more structural detail visible. The particles show the same variations in projectional shape. Some high density areas are seen in the projectional interiors of the particles. Thin segments of slightly lower density may be observed connecting these areas to others on or near the particle edge. When the LDL are cryopreserved at higher concentrations (1.0 mg/ml protein), are observed in thin ice, or are densely packed, they often assume a more angular appearance, sometimes presenting a rounded rectangular projection (Figs. 1–3). These particles are of a more uniform density than their rounder counterparts and exhibit what appears to be a horizontal banding pattern of three to four thin, beaded strands of higher density along the longer axis of the "rectangle." These particles become more prevalent as the preparation ages in storage before freezing.

A set of 337 images was generated by windowing from the ~10 Å/pixel, digitized micrographs of unlabeled LDL. Ovoid-to-circular LDL were windowed preferentially over "rectangular" particles (see above) because the former structure was more common and less likely to reflect interparticle interactions. Fig. 4 presents a montage of 16 typical individual images from this set. The size profile of the particles (Fig. 5) in the 337-image set reveals a mean radius of 116.7 ± 6.4 Å with all radii between 100 and 130 Å, and 90.8% of radii between 110 and 120 Å.

Gold-labeled LDL

Fig. 6 *a* shows fields of Nanogold in vitreous ice at varying defocus. The gold clusters are best visualized at 500 nm

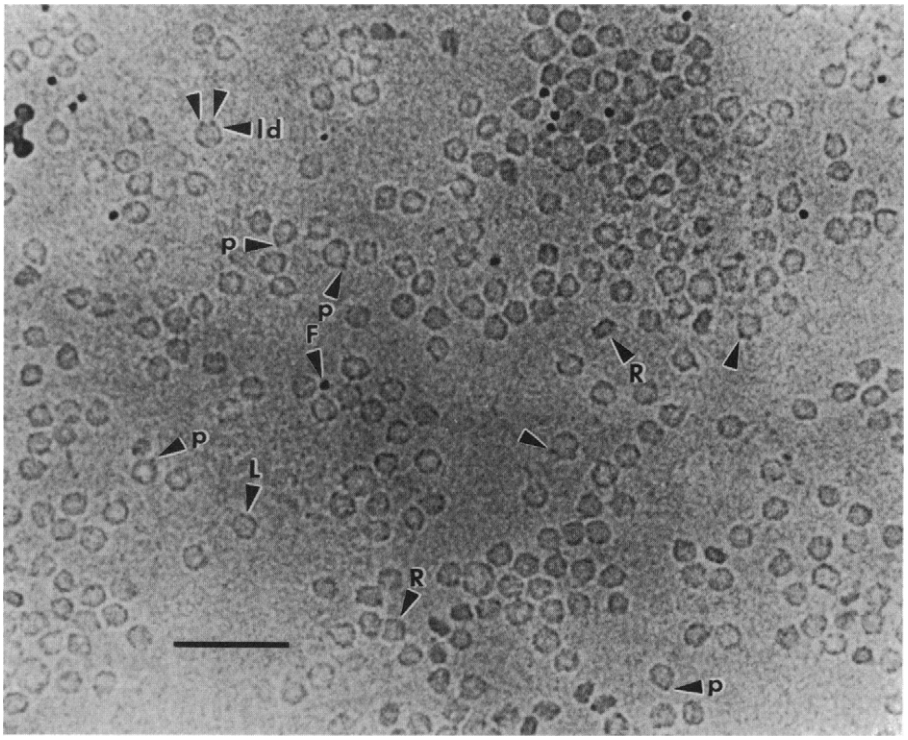

FIGURE 1 Unlabeled LDL particles in vitreous ice. Exposure taken at 49 kX at 2.00 μm defocus in the EM420 (see Materials and Methods). Bar shows 100 nm. (L) LDL particle; (F) ferritin complex; (*plain arrow*) high density region; (p) high density region at "pointed-end" of particle; (ld) lower density connecting region; (R) "rectangular" LDL particle.

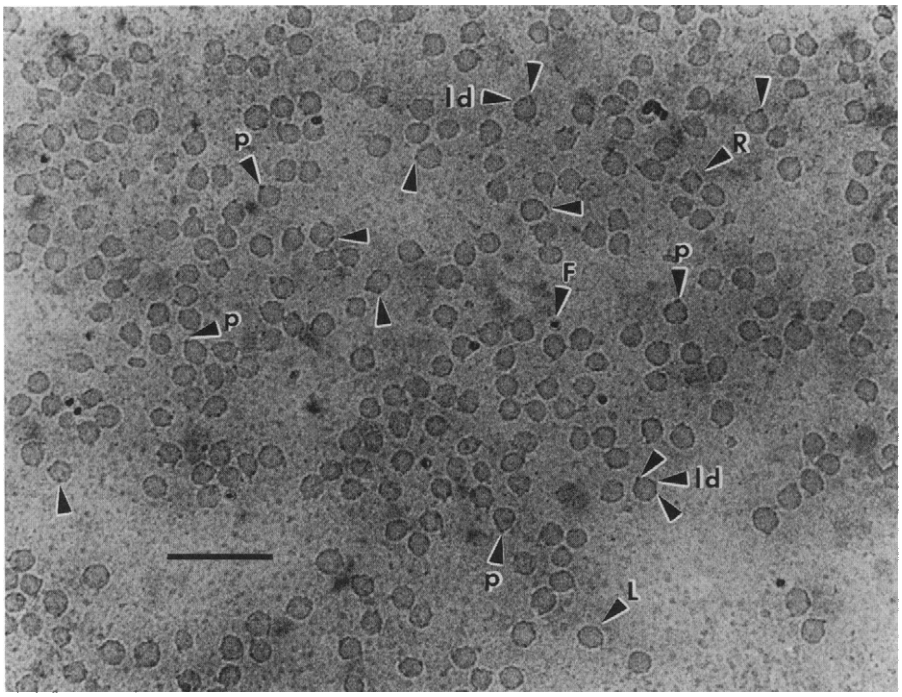

FIGURE 2 Unlabeled LDL particles in vitreous ice. Exposure taken at 60 kX at 2.00 μm defocus in the CM12 (see Materials and Methods). Bar shows 100 nm. (L) LDL particle; (F) ferritin complex; (*plain arrow*) high density region; (p) high density region at "pointed-end" of particle; (ld) lower density connecting region; (R) "rectangular" LDL particle.

defocus and become less defined as defocus increases, but they are still visible at 2.00 μm defocus. Fig. 6 *b* shows fields of gold-labeled LDL at three defocus levels. LDL is well visualized at 2.00 μm defocus and rapidly becomes indistinguishable from background as defocus decreases. A compromise defocus of 1.75 μm was selected to maximize the visualization of both Nanogold and LDL. At this defocus, gold clusters are visible clearly on many particles. In addition, some free gold clusters are visible. The number of gold clusters associated with LDL particles varies from 0 to 2 per LDL, with 1 being more prevalent than 2. Fig. 6 *c* shows a montage of eight images of gold-labeled LDL, scanned, windowed, and masked (see Materials and Methods). Gold clusters are usually distinguishable from the high density areas of the LDL particle, being darker (more dense) and more uniform in shape and size. Gold clusters are seen often on the LDL particle edge, but may be observed also in the interior of LDL particle projections. When two gold clusters label one LDL particle, the distance between them in projection varies from overlapping to approximately 120 Å apart.

The appearance of the LDL particles is similar to that of the unlabeled particles. No visible global structural changes occur as a result of gold labeling. When the LDL particles are "egg-shaped" in projection, the gold clusters are distant from the pointed end, usually 120–180° away.

A set of 1257 images of gold-labeled LDL was generated as above. Fig. 7 shows the size profile of these particles. All LDL were between 100 and 155 Å radius, with mean radius 122.5 ± 9.6 Å and 80.09% of radii within 110–130 Å. Note that the two 14-Å gold clusters (often located at the LDL particle edge) may increase the apparent particle radius. The images at the large extreme (145-Å radius and above) were removed from the set. Most of these images were from one micrograph and possibly were flattened out by the overly thin ice, as suggested by light meter readings. The final set consisted of 1217 images, with a mean radius of 121.7 ± 8.6 Å and 83.6% of radii within 110–130 Å (see Fig. 7).

DISCUSSION

In this study, cryoelectron microscopy and image processing techniques have been developed to visualize the LDL particle and the organization of apo-B100 at the surface of human LDL. Our images show that LDL projections in vitreous ice are slightly ovoid, consistent with several studies demonstrating a quasi-spherical morphology for the LDL particle (Forte and Nichols, 1972; Atkinson et al., 1977; Laggner and Muller, 1978). The average diameters of 233 and 243 Å for unlabeled and gold-labeled LDL, respectively, are in excellent agreement with hydrodynamic (Scanu, 1972) and x-ray small angle scattering measurements (Atkinson et al., 1977).

Some distortion in particle shape accompanied particles located in very thin ice or in close apposition (see Results). A variant on the ovoid structure is observed that is more rectangular in projection, with rounded sides. Three to four beaded threads of high density traverse the particle in parallel along the long axis of the projection. The dimensions (180×200 Å) of these particles are somewhat smaller than ovoid LDL. This morphology is observed under conditions where the LDL particles are tightly packed, the ice is nonvitreous (cubic, hexagonal, etc.), the ice is especially thin, or the LDL preparation becomes aged. The phenomenon becomes more pronounced as the preparation ages. These observations suggest that these particles represent an ultrastructural rearrangement, which may represent a dehydrated or deformed version of the particle because they appear more

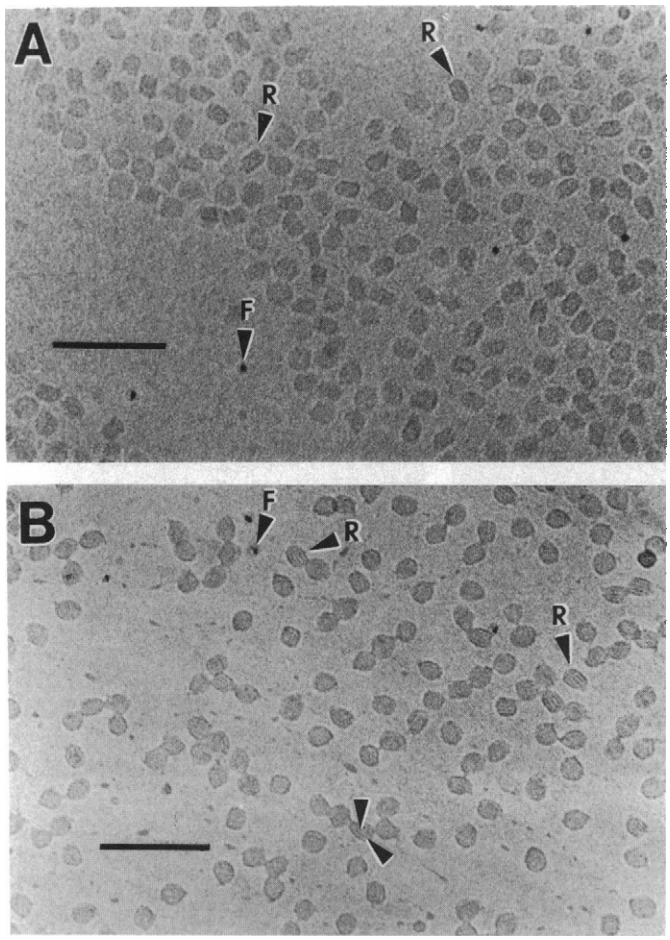

FIGURE 3 (*A*) Densely packed, unlabeled LDL particles in thin vitreous ice. Relative ice thickness was measured using the light meter of the microscope. (*B*) Aged, unlabeled LDL particles in vitreous ice. This sample was cryopreserved 3 months after LDL isolation. Exposures taken at 60 kX at 2.00 μm defocus in the CM12 (see Materials and Methods). Bars show 100 nm; (F) ferritin complex; (R) "rectangular" LDL particle; (*plain arrow*) longitudinal "beaded thread" of density.

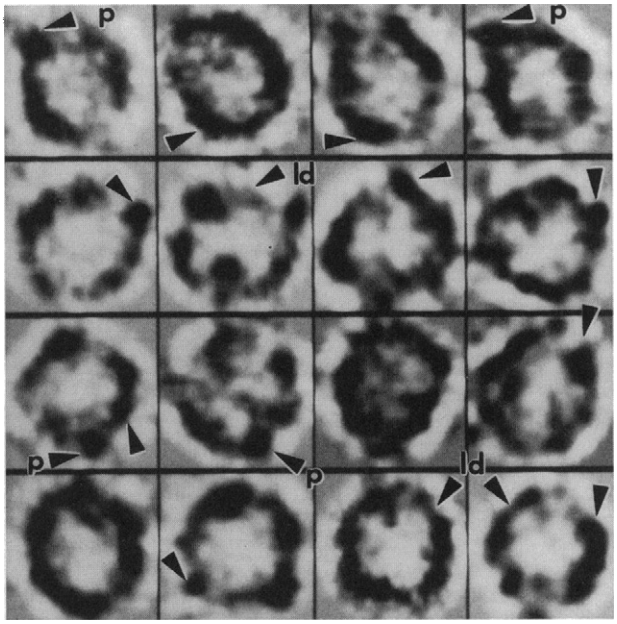

FIGURE 4 Montage of 16 individual, representative images of LDL in vitreous ice. Exposure taken at 49 kX at 2.00 μm defocus in the EM420. Particle images were windowed, masked, and padded (see Materials and Methods) from micrographs that were scanned and digitized at 10 Å/pixel. Images are unfiltered. Each image box is 270×270 Å. Images were translationally centered, and the images in each row were rotationally aligned in real and Fourier space (see Materials and Methods); (*plain arrow*) high density region; (p) high density region of "pointed end" of particle; (ld) lower density "connecting" region.

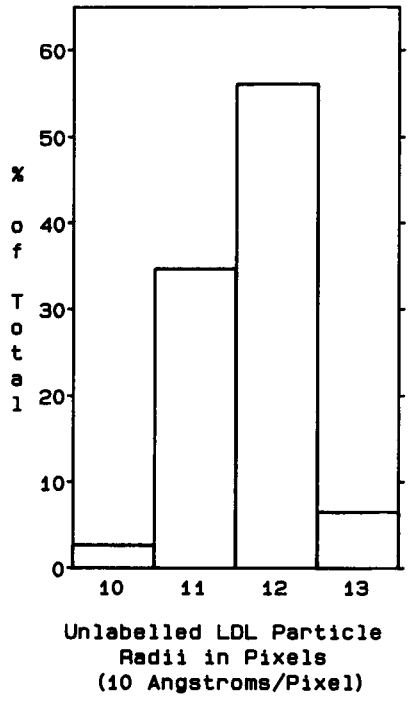

FIGURE 5 Size profile for unlabeled LDL. Exposures were taken at 49 kX at a defocus of 2.00 μm in the EM420 (see text). 480 particles were scanned and digitized from micrographs using a raster with a resolution of ~10 Å/pixel. Deformed and overlapping images were removed from the 480-image set to form a 337-image set. For the 337-image set: mean radius 11.67 ± 0.64 pixels (116.7±6.4Å), with 90.8% within 110- to 120-Å radius. All images were within 100- to 130-Å radius.

often in areas where they are poorly hydrated (thin ice, tight packing, nonvitreous ice).

Individual images of LDL exhibit discrete high density regions that probably represent apo-B100. These regions are connected by distinguishable regions of slightly lower density at the edge of LDL particle projections. Although most apoB is visible at the edge of projections, it may be seen simultaneously in the interiors of the projections. Thin strings of high density sometimes connect the inner and outer regions. Negative stain EM studies of apoB extracted from LDL indicate that the protein forms a ring of variable thickness (Phillips and Schumaker, 1989), which has been interpreted to suggest that apoB exists on the LDL surface as a protein belt (Chatterton et al., 1991; Phillips and Schumaker, 1989). Our images suggest a more distributed and complicated surface organization in which apoB appears to meander considerably over the particle surface, with discrete domains connected by more extended strands of protein. The images show large areas of high density material that may represent

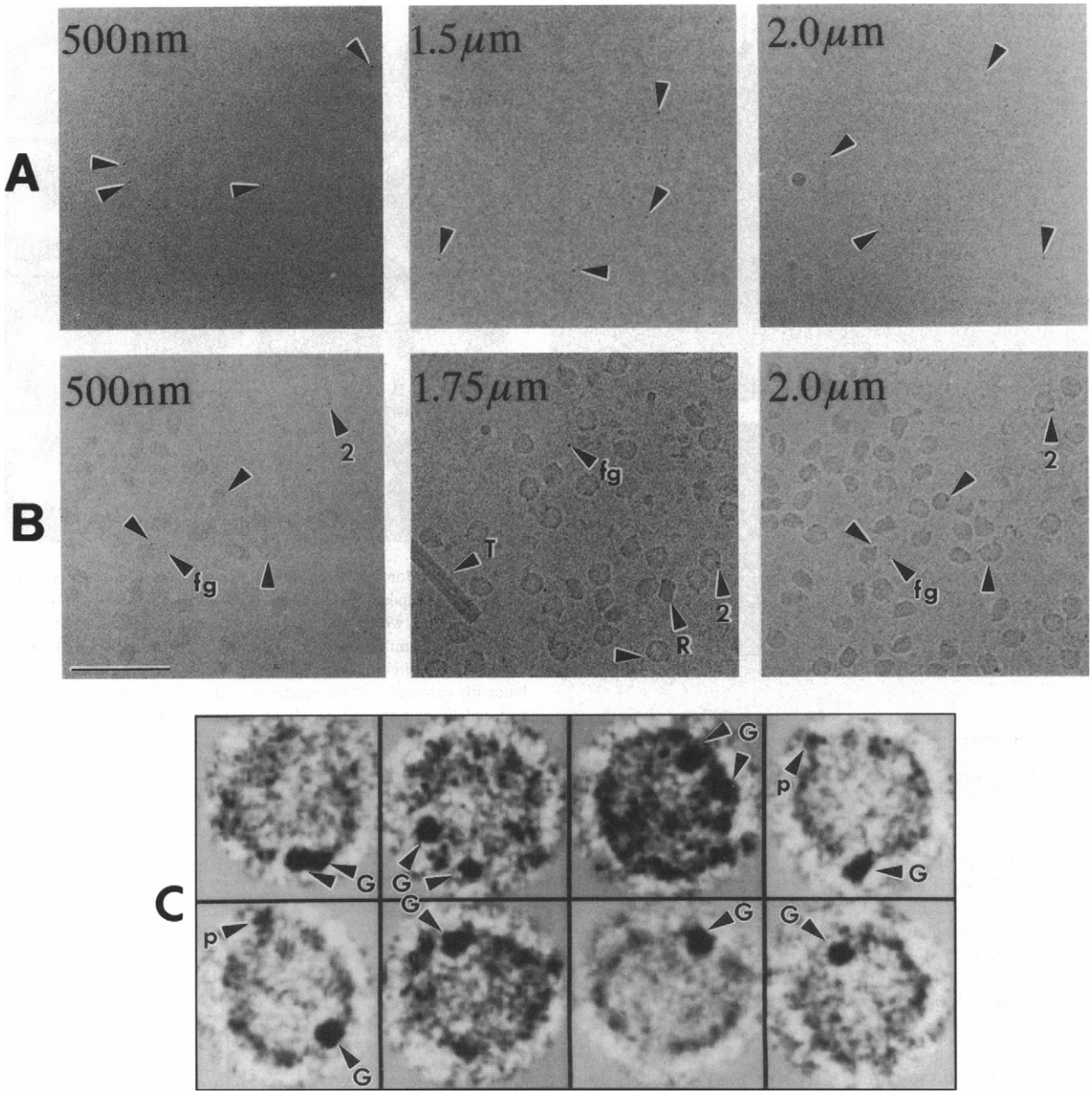

FIGURE 6 (*A*) Nanogold at varying defocus in vitreous ice. Exposures taken at 60 kX in the CM12. Defocus levels are as labeled. Bar (*B*) shows 100 nm. Visualization of gold clusters decreases with increasing defocus, from left to right. (*plain arrow*) Nanogold cluster. (*B*) Nanogold-LDL at varying defocus in vitreous ice. Exposures taken at 60 kX in the CM12. Defocus levels are as labeled. Bar shows 100 nm. Visualization of gold clusters decreases with increasing defocus, from left to right. Visualization of LDL particles increases with increasing defocus. (*plain arrow*) Nanogold cluster on LDL particle; (fg) free gold cluster; (2) two gold clusters labeling one LDL particle; (R) "rectangular" LDL particle; (T) tobacco mosaic virus. (*C*) Nanogold-LDL at 1.75 μm defocus in vitreous ice. Exposures taken at 60 kX in the CM12. Particle images were windowed, masked, and padded (see Materials and Methods) from micrographs that were scanned and digitized using a raster with resolution ~5 Å/pixel. Images are unfiltered. Each image box is 300×300 Å; (G) Nanogold cluster on LDL particle. Each arrow corresponds to one gold cluster; (p) high density region at "pointed-end" of LDL particle. Connecting regions of lower density are visible in all images.

protein superdomains linked by lower density areas (Atkinson, 1988; Spin and Atkinson, 1993). Some of the putative domains are approximately circular in projection, whereas one appears quite elongated. There are gaps of varying density between the domains bridged by thinner areas of density that are less globular in appearance.

Several studies have discussed the number of structural domains that make up apoB-100 on LDL (Brown and Goldstein, 1984; Chatterton et al., 1991; Chen et al., 1989; Gulik-Kryzwicki et al., 1979; Lee et al., 1987; Luzzati et al., 1979; Phillips and Schumaker, 1989; Pollard et al., 1969; Walsh and Atkinson, 1990; Yang et al., 1989). Limited trypsin proteolysis studies of apoB on LDL have suggested that apoB is divided into five domains (Yang et al., 1989). Differential scanning calorimetry (DSC) data (Walsh and Atkinson, 1990) for apoB solubilized in NaDC also indicate four to five

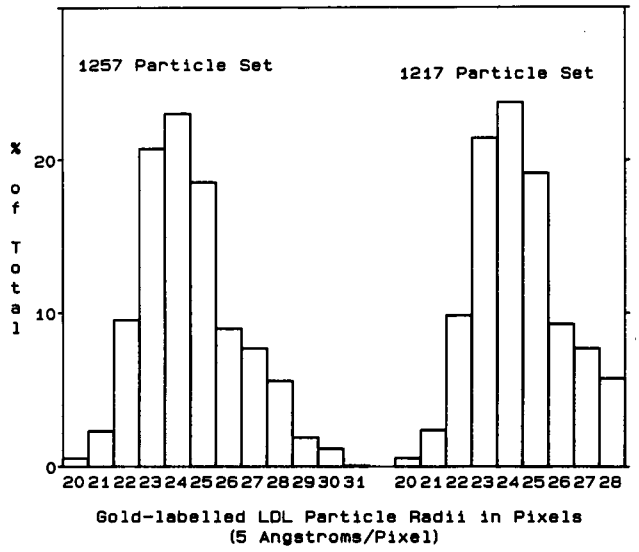

FIGURE 7 Size profiles for Nanogold-labeled LDL. Exposures taken at 60 kX at a nominal defocus of 1.75 μm in the CM12 (see text). 1257 particles were scanned and digitized using a raster with resolution ~5 Å/pixel. 24 of 40 particles removed to form a 1217-particle set were from one micrograph. For the 1257-image set: mean radius 24.5 ± 1.9 pixels (122.5 ± 9.6 Å), with 80.09% within 110- to 130-Å radius. For the 1217-image set: mean radius 24.3 ± 1.7 pixels (121.7 ± 8.6 Å), with 83.6% within 110- to 130-Å radius.

structural domains that undergo independent reversible thermal unfolding. Fourier power spectrum (FPS) analysis of apoB sequence amphipathicity reveals that the protein is divided into five domains of secondary structure prevalence (Nolte, 1994). The domains alternate N-$\alpha\beta\alpha\beta\alpha$-C, and the residues present in each are similar to those delineated by Yang et al. (1989).

The unlabeled LDL images obtained on the CM12 are similar to those obtained from the EM420, and improved contrast reveals more detail. The images from the CM12 show that the protein layer clearly displays the "beaded-thread" appearance of apoB. The most dense region of the protein is located at the pointed end in ovoid projections. This dense region may represent the N-terminal region (residues 1–1000, Domain I) (Yang et al., 1989). This region is the most easily released on trypsin digestion and is also the most hydrophilic region of the protein (Cladaras et al., 1986), and it may not be strongly associated with the lipid core of LDL.

Chatterton et al., using negative stain immunoelectron microscopy, mapped several monoclonal antibodies with epitopes within the first 1082 residues of apoB fairly close together with respect to the overall particle, within 45° of each other (12.5% of the LDL circumference). However, their data show large discrepancies between the diameter of LDL from EM (~285 Å) and the hydrodynamically determined size (~208 Å) that might represent a deformation of the LDL particles during drying in the negative staining process (Chatterton et al., 1991; Phillips and Schumaker, 1989; Shen et al., 1981).

The elongated domain seen in the images is the largest domain, and may therefore represent Domain III (residues 1701–3070) (Yang et al., 1989). Chatterton et al. mapped epitope residues 2488–2658 87–122° from N-terminal domain epitopes. Our LDL images reveal that the elongated domain is approximately 50–140° distant from the "pointed-end" domain in ovoid projections.

Studies of pyruvate and 2-oxoglutarate dehydrogenase have used Nanogold to enhance site-specific visualization by cryoelectron microscopy (Wagenknecht et al., 1992). The 14-Å gold clusters were clearly resolved in frozen-hydrated complexes. Because apoB has only two surface-exposed sulfhydryls (Coleman et al., 1989; Sommer et al., 1991; Yang et al., 1990) and the monomaleimido active portion of Nanogold labels these sites exclusively, this probe provides a unique site-specific label for apoB (Furuya et al., 1991; Hainfeld and Furuya, 1992). In images of gold-labeled LDL, the gold clusters are clearly visibly on the particles.

Images of Nanogold-labeled LDL particles commonly show one gold cluster rather than than two. Cys-24 (residue 4190) on apoB has been shown to have less surface exposure than Cys-22 (residue 3734) (Coleman et al., 1989; Sommer et al., 1991; Yang et al., 1990). Cys-22 was identified recently as the residue that forms the disulfide linkage with Cys4057 of apo(a), substantiating its surface availability (Guevara et al., 1993). Because Cys-22 is more accessible, it may be labeled preferentially by Nanogold.

The gold clusters on gold-labeled LDL are observed fairly distant from the "pointed-end" domain in the ovoid projections. The epitopes of two antibodies used in the studies of Chatterton et al. bracket the location of Cys-22. In addition, the epitope to one of these antibodies is located one residue N-terminal to Cys-24. The binding sites of these antibodies mapped 82–140° away from the three N-terminal antibodies. In the "egg-shaped" images of LDL, lone gold clusters are located approximately 120° from the pointed end. When particles were twice-labeled, inter-cluster distances varied depending on view. However, the clusters appeared very close together in "egg-shaped" projections. It is likely that the domain containing Cys-22 and Cys-24 is fairly distant from the "pointed-end" domain.

LDL particles in vitreous exist presumably in no preferred orientation. Therefore, currently we are developing image processing methods including correspondence analysis and classification methodologies (J. Frank et al., 1978, 1985, 1988; Wagenknecht et al., 1988) to select, evaluate, and group the images of LDL and gold-labeled LDL. We are also pursuing antibody-mapping studies in vitreous ice, using IgGs and Fab′ fragments labeled with Nanogold in conjunction with gold-labeled LDL to aid in the image processing (Hainfeld and Furuya, 1992). These studies will include tilted images, allowing us to use three-dimensional reconstruction techniques to elucidate further structural details.

Dr. David Atkinson thanks the Medical Research Council Laboratory for Molecular Biology (Cambridge, U.K.) and, in particular, Dr. Richard Henderson, for the opportunity to begin these studies while on sabbatical. We thank Margaret Gibbons for preparation of the manuscript, Dr. Mary Walsh and Joan Richmond for help with isolation and characterization of LDL, and Dr. Donna Cabral-Lilly for help and instruction in cryo-EM techniques.

This work was supported by grants from National Institutes of Health, research grant HL26335, and Training grant GM08291.

REFERENCES

Adrian, M., J. Dubochet, J. Lepault, and A. W. McDowall. 1984. Cryo-electron microscopy of viruses. *Nature.* 308:32–36.

Atkinson, D. 1988. Electron microscopy of unstained frozen hydrated low density lipoprotein. *Arteriosclerosis.* 8:598*a*. (Abstr.)

Atkinson, D., R. J. Deckelbaum, D. M. Small, and G. G. Shipley. 1977. Structure of human plasma low-density lipoproteins: molecular organization of the central core. *Proc. Natl. Acad. Sci. USA.* 74:1042–1046.

Basu, S. K., R. G. W. Anderson, J. L. Goldstein, and M. S. Brown. 1977. Metabolism of cationized lipoproteins by human fibroblasts. *J. Cell Biol.* 74:119–135.

Brown, M. S., and J. L. Goldstein. 1976. Receptor-mediated control of cholesterol metabolism. *Science.* 191:150–154.

Brown, M. S., and J. L. Goldstein. 1984. How LDL receptors influence cholesterol and atherosclerosis. *Sci. Am.* 251:58–66.

Cardin, A. D., K. R. Witt, J. Chao, H. S. Margolius, V. H. Donaldson, and R. L. Jackson. 1984. Degradation of apolipoprotein B-100 of human plasma low density lipoproteins by tissue and plasma kallikreins. *J. Biol. Chem.* 259:8522–8528.

Chatterton, J. E., M. L. Phillips, L. K. Curtiss, R. W. Milne, Y. L. Marcel, and V. N. Schumaker. 1991. Mapping apolipoprotein B on the low density lipoprotein surface by immunoelectron microscopy. *J. Biol. Chem.* 266: 5955–5962.

Chen, G. C., S. Zhu, D. A. Hardmann, J. W. Schilling, K. L. Lau, and J. P. Kane. 1989. Structural domains of human apolipoprotein B-100. Differential accessibility to limited proteolysis of B-100 in low density and very low density lipoproteins. *J. Biol. Chem.* 264:14369–14375.

Cladaras, C., M. Hadzopoulou-Cladaras, R. T. Nolte, D. Atkinson, and V. I. Zannis. 1986. The complete sequence and structural analysis of human apolipoprotein B-100: relationship between apoB-100 and apoB-48 forms. *EMBO J.* 5:3495–3507.

Coleman, R. D., T. W. Kim, A. M. Gotto, Jr., and C. Y. Yang. 1989. Determination of cysteine on low-density lipoproteins using the fluorescent probe, 5-iodoacetamidofluoresceine. *Biochim. Biophys. Acta.* 1037:129–132.

Deckelbaum, R. J., G. G. Shipley, D. M. Small, R. S. Lees, and P. K. George. 1975. Thermal transitions in human plasma low density lipoproteins. *Science.* 190:392–394.

Dubochet, J., M. Adrian, J.-J. Chang, J.-C. Homo, J. Lepault, A. W. McDowall, and P. Schultz. 1987. Cryo-electron microscopy of vitrified specimens. *Q. Rev. Biophys.* 21:129–228.

Erickson, H. P., and A. Klug. 1971. Measurement and compensation of defocusing and aberrations by Fourier processing of electron micrographs. *Phil. Trans. R. Soc. Lond.* 261:105–118.

Forte, T., and A. V. Nichols. 1972. Application of electron microscopy to the study of plasma lipoprotein structure. *Adv. Lipid Res.* 10:1–41.

Frank, J., J.-P. Bretaudiere, J.-M. Carazo, A. Verschoor, and T. Wagenknecht. 1988. Classification of images of biomolecular assemblies: a study of ribosomes and ribosomal subunits of *Escherichia coli*. *J. Microsc. (Oxford).* 150:99–115.

Frank, J., W. Goldfarb, D. Eisenberg, and T. S. Baker. 1978. Reconstruction of glutamine synthetase using computer averaging. *Ultramicroscopy.* 3:283–290.

Frank, J., B. Shimkin, and H. Dowse. 1981. SPIDER — a modular software system for electron image processing. *Ultramicroscopy.* 6:343–358.

Frank, J., A. Verschoor, and T. Wagenknecht. 1985. Computer processing of electron microscopic images of single macromolecules *In* New Methodologies in Studies of Protein Configuration. T. T. Wu, editor. van Nostrand Reinhold, New York. 36–39.

Furuya, F. R., J. F. Hainfeld, and R. D. Powell. 1991. A new 1.4 nm gold Fab′ probe. EMSA 49 Annual Meeting, Proc., Poster #PB 14.

Ginsburg, G. S., D. M. Small, and D. Atkinson. 1982. Microemulsions of phospholipids and cholesterol esters: protein-free models of low density lipoproteins. *J. Biol. Chem.* 257:8216–8227.

Gofman, J. W., L. Rubin, J. P. McGinley, and H. B. Jones. 1954. Hyperlipoproteinemia. *Am. J. Med.* 17:514–520.

Guevara, J., Jr., J. Spurlino, A. Y. Jan, C. Y. Yang, A. Tulinsky, B. V. V. Prasad, J. W. Gaubatz, and J. D. Morrisett. 1993. Proposed mechanisms for binding of apo kringle type 9 to apo B-100 in human lipoprotein . *Biophys. J.* 64:686–700.

Gulik-Kryzwicki, T., M. Yates, and L. P. Aggerbeck. 1979. Structure of serum low density lipoprotein II. A freeze-etching electron microscopy study. *J. Mol. Biol.* 131:475–484.

Hainfeld, J. F., and F. R. Furuya. 1992. A 1.4 nm gold cluster covalently attached to antibodies improves immunolabeling. *J. Histochem. Cytochem.* 40:177–184.

Havel, R. J., J. A. Elder, and J. H. Bragdon. 1955. The distribution and chemical composition of ultracentrifugally separated lipoproteins in human serum. *J. Clin. Invest.* 34:1345–1353.

Kannel, W. B., W. P. Castelli, T. Gordan, and P. M. McNamara. 1971. Serum cholesterol, lipoproteins, and the risk of coronary heart disease. The Framingham study. *Ann. Intern. Med.* 74:1–12.

Knott, T. J., L. M. Pease, L. M. Powell, S. C. Wallis, S. C. Rall, Jr., T. L. Innerarity, B. Blackhart, W. H. Taylor, Y. Marcel, R. Milne, D. Johnson, M. Fuller, A. J. Lusis, B. J. McCarthy, R. W. Mahley, B. Levy-Wilson, and J. Scott. 1986. Complete protein sequence and identification of structural domains of human apolipoprotein B. *Nature.* 323:734–738.

Laggner, P., and K. W. Muller. 1978. The structure of serum lipoproteins as analyzed by x-ray small-angle scattering. *Q. Rev. Biophys.* 11:371–425.

Lee, D. M., D. L. Stiers, and T. Mok. 1987. Apolipoprotein B is a globular protein — morphological studies by electron microscopy. *Biochem. Biophys. Res. Commun.* 144:210–216.

Lepault, J., F. P. Booy, and J. Dubochet. 1983. Electron microscopy of frozen biological suspensions. *J. Microsc. (Oxford).* 129:89–102.

Lowry, O. H., N. J. Rosebrough, A. L. Farr, and R. J. Randall. 1951. Protein measurement with the Folin phenol reagent. *J. Biol. Chem.* 193:265–275.

Luzzati, V., A. Tardieu, and L. P. Aggerbeck. 1979. Structure of serum low density lipoprotein I. A solution x-ray scattering study of a hyperlipidemic monkey low density lipoprotein. *J. Mol. Biol.* 131:435–473.

Mahley, R. W., and T. L. Innerarity. 1978. Sixth International Symposium on Drugs Affecting Lipid Metabolism. D. Kritchevsky, R. Paoletti, and W. L. Holmes, editors. Plenum Press, New York. 99–127.

Milligan, R. A., A. Brisson, and P. N. T. Unwin. 1984. Molecular structure determination of crystalline specimens in frozen aqueous solutions. *Ultramicroscopy.* 13:1–10.

Noble, R. P. 1968. Electrophoretic separation of plasma lipoproteins in agarose gel. *J. Lipid Res.* 9:693–700.

Nolte, R. T. 1994. Structural analysis of the human apolipoproteins: an integrated approach utilizing physical and computational methods, Vol. I and II. Ph.D. Thesis. Biochemistry Department, Boston University School of Medicine. University Microfilms Inc., #93–32587.

Owen, C., and D. DeRosier. 1993. A 13 Å map of the actin-scruin filament from the limulus acrosomal process. *J. Cell Biol.* 123:337–344.

Peterson, G. L. 1979. Review of the Folin phenol protein quantitation method of Lowry, Rosebrough, Farr and Randall. *Anal. Biochem.* 100: 201–220.

Phillips, M. L., and V. N. Schumaker. 1989. Conformation of apolipoprotein B after lipid extraction of low density lipoproteins attached to an electron microscope grid. *J. Lipid Res.* 30:415–422.

Pollard, H., A. M. Scanu, and E. W. Taylor. 1969. On the geometrical arrangement of the protein subunits of human serum low-density lipoprotein: evidence for a dodecahedral model. *Proc. Natl. Acad. Sci. USA.* 64:304–310.

Redgrave, T. G., D. C. K. Roberts, and C. E. West. 1975. Separation of plasma lipoproteins by density-gradient ultracentrifugation. *Anal. Biochem.* 65:42–49.

Scanu, A. M. 1972. Structural studies on serum lipoproteins. *Biochim. Biophys. Acta.* 265:471–508.

Shen, M. M. S., R. M. Krauss, F. T. Lindgren, and T. Forte. 1981. Heterogeneity of serum low density lipoproteins in normal human subjects. *J. Lipid Res.* 22:236–244.

Sniderman, A., S. Shapiro, D. Marpole, B. Skinner, B. Teng, and P. O. Kwiterovich, Jr. 1980. Association of coronary atherosclerosis with hyperapobetalipoproteinemia [increased protein but normal cholesterol levels in human plasma low density (β) lipoproteins]. *Proc. Natl. Acad. Sci. USA.* 77:604–608.

Sommer, A., R. Gorges, G. M. Kostner, F. Paltauf, and A. Hermetter. 1991. Sulfhydryl-selective fluorescence labeling of lipoprotein(a) reveals evidence for one single disulfide linkage between apoproteins(a) and B-100. *Biochemistry.* 30:11245–11249.

Spin, J. M., and D. Atkinson. 1993. Structure of low density lipoprotein in vitreous ice. *Biophys. J.* 64:286*a*. (Abstr.)

Wagenknecht, T., R. Grassucci, J. Berkowitz, K. Carbone, F. Furuya, and J. Hainfeld. 1992. Electron microscopy of unstained gold-cluster labeled pyruvate and 2-oxoglutarate dehydrogenase complexes. *Biophys. J.* 61: 2705. (Abstr.)

Wagenknecht, T., R. Grassucci, and J. Frank. 1988. Electron microscopy and computer image averaging of ice-embedded large ribosomal subunits from *Escherichia coli*. *J. Mol. Biol.* 199:137–147.

Wagenknecht, T., R. Grassucci, and D. Schaak. 1990. Cryoelectron microscopy of frozen hydrated α-ketoacid dehydrogenase complexes from *Escherichia coli*. *J. Biol. Chem.* 265:22402–22408.

Walsh, M. T., and D. Atkinson. 1990. Calorimetric and spectroscopic investigation of the unfolding of human apolipoprotein B. *J. Lipid Res.* 31:1051–1062.

Yang, C.-Y., S.-H. Chen, S. H. Gianturco, W. A. Bradley, J. T. Sparrow, M. Tanimura, W.-H. Li, D. A. Sparrow, H. DeLoof, M. Rosseneu, F.-S. Lee, Z.-W. Gu, and A. M. Gotto, Jr. 1986. Sequence, structure, receptor-binding domains and internal repeats of human apolipoprotein B-100. *Nature.* 323:738–742.

Yang, C.-Y., Z.-W. Gu, S.-A. Weng, T. W. Kim, S.-H. Chen, H. J. Pownall, P. M. Sharp, S.-W. Liu, W.-H. Li, A. M. Gotto, Jr., and L. Chan. 1989. Structure of apolipoprotein B-100 of human low density lipoproteins. *Arteriosclerosis.* 9:96–108.

Yang, C.-Y., T. W. Kim, S.-A. Weng, B. Lee, M. Yang., and A. M. Gotto, Jr. 1990. Isolation and characterization of sulfhydryl and disulfide peptides of human apolipoprotein B-100. *Proc. Natl. Acad. Sci. USA.* 87: 5523–5527.